Hierarchically assembled tubular shell-core-shell heterostructure of hybrid transition metal chalcogenides for high-performance supercapacitors with ultrahigh cyclability

Young-Woo Lee,[‡a] Byung-Sung Kim,[‡a] John Hong,[a] Heechae Choi,[b] Hyun-Sik Jang,[c] Bo Hou,[a] Sangyeon Pak,[a] Juwon Lee,[a] Sang-Hyo Lee,[a] Stephen M. Morris,[a] Dongmok Whang,[c] JinPyo Hong,[d] Hyeon Suk Shin,[e] SeungNam Cha,*[a] Jung Inn Sohn*[a] and Jong Min Kim[f]

[a] Department of Engineering Science, University of Oxford, Oxford OX1 3PJ, UK
[b] Center for Computational Science, Korea Institute of Science and Technology, Seoul 02792, Republic of Korea
[c] School of Advanced Materials Science and Engineering, SKKU Advanced Institute of Nanotechnology (SAINT), Sungkyunkwan University, Gyeonggi-Do 16419, Republic of Korea
[d] Research Institute of Convergence of Basic Science, Novel Functional Materials and Device Laboratory, Department of Physics, Hanyang University, Seoul 15588, Republic of Korea
[e] Department of Chemistry, Ulsan National Institute of Science and Technology (UNIST), Ulsan 44919, Republic of Korea
[f] Electrical Engineering Division, Department of Engineering, University of Cambridge, Cambridge CB3 0FA, UK

‡ These authors contributed equally to this work.

* Corresponding author. Tel: +44-1865-273912. Fax: +44-1865-273010.

E-mail address: seungnam.cha@eng.ox.ac.uk (Prof. S.N. Cha); junginn.sohn@eng.ox.ac.uk (Dr. J.I. Sohn)

ABSTRACT

Pseudo-capacitive transition metal chalcogenides have recently received remarkable attention as promising electrode materials for supercapacitors (SCs) because they have efficient Faradic redox reactions and good electrical conductivity, allowing energy storage capability with an order of magnitude greater than that of conventional carbon-based materials. However, the important challenge associated with utilization of such high-capacitive electrode materials remains improving their capacity retention with the long-term cycling stability. Here, we propose a novel heteroatom transition metal (Cu-Ni) chalcogenide core-shell (HTMC-CS) hollow tubular structure directly grown on a Cu mesh current collector using a hierarchical bottom-up synthetic approach. The resultant HTMC-CS electrode exhibits outstanding pseudo-capacitive behaviors, such as the high areal capacitance of 700 mF cm^{-2} and the high volumetric capacitance of 25.9 F cm^{-3} at a current density of 2 mA cm^{-2}. Furthermore, the asymmetric SCs based on the active carbon anode and the HTMC-CS cathode show the high power (770 mW cm^{-3}) and energy (2.63 mWh cm^{-3}) densities as well as the ultrahigh reversible capacity with the capacitance retention of 84% and the long-term cycling stability over 10000 cycles. These remarkably improved electrochemical features are discussed and explained by the unique combination of CuS core and NiS shell materials and their hierarchical hollow tubular geometry with an optimized inner/outer shell structure and an mechanical stress-mitigating interlayer, allowing highly reversible and efficient electrochemical redox processes coupled with fast charge transfer kinetics and electrochemically stable structure.

Keywords: Transition metal, Chalcogenide, Core-shell; Nanoarchitecture, Supercapacitor

INTRODUCTION

The recent rapid pace of technological advances in areas of electrical vehicles, high energy consuming portable electronics, and energy back-up systems for emergency and unbalanced power supplies during day and night, has triggered tremendous efforts to develop an innovative energy storage system for future success in world-wide efforts on meeting the ever-increasing demands for high energy and power density concerns.[1,2] In this regard, supercapacitors (SCs) that can electrochemically store charge and deliver energy with high power density and ultrahigh reversible cyclability have become crucial as one of the most promising energy storage systems to complement or replace batteries.[3] Particularly, pseudo-capacitive SCs, which are operated through reversible Faradic redox mechanism, essentially require electrode materials with various valance states, good electrical conductivity, large surface areas. Therefore, many efforts have been devoted to seeking for suitable pseudo-capacitive materials with the desirable Faraday redox balance, such as transition metal based oxide/hydroxide, by considering the design of novel electrodes with hierarchical structures to synergistically maximize the active surface areas, charge transport kinetics, and the cycle stability.[4] As a result, it is highly expected to attain the superior pseudo-capacitive behaviors such as high specific capacitance and high rate-performance as well as the ultrahigh cyclability during the charge/discharge process.

Recently, as a new type of emerging pseudo-capacitive materials, transition metal chalcogenides, such as CoS,[5] SnS,[6] ZnS,[7] and MnS,[8] have been considered and investigated for next-generation pseudo-capacitive SCs. Among them, a nickel chalcogenide (NiS) has been demonstrated to be a quite promising candidate for pseudo-capacitive electrodes since it has the superior intrinsic electrical conductivity and the high specific capacitance based on the active Faradic redox reaction of Ni^{2+}/Ni^{3+}, resulting in the enhanced energy density.[9-12] However, it has been reported that the NiS electrode exhibits the nature of serious capacity fading because of its low

structural stability induced by the electrosorption and intercalation reaction process, which produces the acute internal mechanical stress during the charge-discharge cycling.[9] To date, there have been several investigations to address the issues of NiS structural instability related to the long-term cyclability by introducing different approaches, such as electrode-structure engineering and hybrid electrodes combined with other transition metal oxides/chalcogenide materials or nanostructured carbon materials.[11-13] However, it is still challenging but highly desirable to develop an effective and practical strategy to achieve excellent electrochemical performances without sacrificing the stability of electrode structure.

Very recently, we showed great promise towards the excellent electrochemical cyclability and good structural stability of pseudo-capacitive SCs by successfully synthesizing the well-arrayed copper chalcogenide (CuS) nanowires with the excellent electrical conductivity and good crystallinity as well as the good electrical contact to a Cu mesh current collector.[14] Based on our previous study, we here report a new approach to design and develop novel hierarchical heteroatom transition metal (Cu and Ni) chalcogenide core-shell (HTMC-CS) electrode materials, consisting of the electrochemically stable CuS hollow nanotube as a core structure and the superior pseudo-capacitive NiS nanoscale-thin layer as an inner/outer shell structure, directly grown on a Cu mesh current collector via a free-standing growth method. Particularly, we carefully selected and designed the combination of two different typical metal chalcogenide materials for hierarchical core-shell SC electrodes by considering various parameters which are important factors to evaluate the feasibility of such an electrode as fitted in a radar plot of Fig. 1a.[15-19] In spite of the relatively low capacitance of CuS electrode materials, their superior electrical conductivity, good rate property, and high structural stability as well as their low cost make them promising materials for the use as the core material, leading to the superior long-term stability under the electrochemical cycling conditions. NiS electrode materials, on the other hand, exhibit the excellent capacitive properties

due to their electrochemically superior reactivity with the OH^- ions. Thus, the novel hierarchical HTMC-CS electrode architecture in combination with utilizing each beneficial structural and electrochemical feature is systematically designed to simultaneously demonstrate the excellent cyclability and energy storage capability, as illustrated in Fig. 1b. First, the nanoscale NiS shell layer on the inner/outer surface of the hollow tubular core structure allows for the enhanced areal capacitance and the shortened ion diffusion distance, inducing the improved energy density. Second, the directly grown HTMC-CS electrodes with highly conductive CuS core materials on the current collector not only provide a favorable conductive pathway for efficient charge transport but also facilitate fast ion diffusion and facile electrolyte permeation, consequently resulting in the high rate performance and the enhanced power density. Third, the unique hierarchical tubular structures with the well-defined pore space and the energetically stable core-shell intermediate region tolerate possible structural variation and accommodate mechanical stress during the charge/discharge process, contributing to the excellent cyclability. We also demonstrated that the electrochemically pseudo-capacitive characteristics of the HTMC-CS electrode are strongly dependent on the NiS shell layer structure through the investigation of the kinetic relationship between the OH^- ion diffusion behavior and the shell thickness. Finally, we demonstrated the asymmetric supercapacitor (ASC) based on the HTMC-CS, exhibits the superior electrochemical properties including the high maximum energy (2.63 mWh cm^{-3}) with power (770 mW cm^{-3}) densities and the ultrahigh cyclability up to the 10000 cycles that are comparable to the commercial energy storage device.

RESULTS AND DISCUSSION

In order to achieve a well-organized CuS/NiS core-shell structure directly grown on a current collector, $Cu(OH)_2$ nanotubes were first prepared by using a free-stranding growth method so as to employ as template for the production of core CuS nanotube arrays. As shown in scanning

electron microscopy (SEM) images of Fig. 2a, the well-defined hollow structure of 1-dimensional $Cu(OH)_2$ nanotubes was observed. Fig. 2d shows that all the X-ray diffraction (XRD) peaks of the $Cu(OH)_2$ nanotubes correspond to the orthorhombic $Cu(OH)_2$ phase (JCPDS No. 13-0420) and confirm the formation of a highly crystalline structure. And then, the CuS nanotubes were obtained without the specific aggregation among nanostructures and the structural collapse through the sulfurization process based on anion exchange reactions as indicated in Fig. 2b. Moreover, the XRD patterns of a CuS nanotube sample are well indexed to the hexagonal CuS phase (JCPDS No. 06-0464, Figs. 2e and S1a, ESI†). As demonstrated in our previous work, it is highly expected that the crystalline CuS will contribute to the cyclability improvements for SCs due to its excellent structural feature and electrochemical stability. Lastly, to maximize the active sites for pseudo-capacitive reactions, nanoscale NiS shell layers coated on both the whole inner and outer CuS nanotube walls were fabricated through sequential Ni and S species adsorption processes by the dip-coating of the as-produced CuS nanotube as shown in Fig. 2c. It is also clearly confirmed that the synthesized NiS shell is the hexagonal-structured α-NiS phase, as shown by the XRD patterns (JCPDS No. 02-1280) in Figs. 2f and S1b, ESI†.

The detailed morphology and structural features of the HTMC-CS were further investigated using transmission electron microscopy (TEM) as shown in Fig. 3a. It can be seen that the HTMC-CS has the well-defined hollow tubular nanostructure with a pore diameter of ~30 nm and a wall thickness of ~50 nm whereby the tubular wall consists of the inner/outer NiS shells (the light gray region) and the CuS core (the relatively dark region). Furthermore, the energy dispersive X-ray spectroscopy (EDX) line-scanning profiles (Fig. 3b) and the EDX mapping profile (Fig. 3c) obviously confirm that nanoscale thin NiS shell layers (approximately 10-15 nm) are formed on the inner and outer wall of the CuS nanotube. Note that unlike previously reported core-shell nanowires with only a single outer shell layer,[20-22] our unique hierarchical HTMC-CS structures can increase

the utilization of active electrode materials through the inner/outer NiS shell layer structure and can provide the efficient OH^- ion diffusion channel, thereby improving the pseudo-capacitive behavior for high volumetric energy and power densities.

The surface chemical state of the HTMC-CS was determined by X-ray photoelectron spectroscopy (XPS), which reveals that the Cu $2p_{3/2}$ XPS spectrum appears two peaks centered at binding energies of 932.63 eV and 934.02 eV, corresponding to Cu^0 and Cu^{2+} states, respectively (Fig. 3d).[23,24] The Ni $2p_{3/2}$ XPS spectrum was also clearly observed, which can be deconvoluted into two oxidized Ni states with a strong peak at 853.29 eV and a weak peak at 854.90 eV, revealing the presence of Ni-S bond and oxidized Ni states, respectively (Fig. 3e).[23,25] Moreover, it can be seen that the peak of S $2p_{3/2}$ with the binding energy at 162.0 eV corresponds to the combined metal-S bonds (Fig. 3f).[14,23] These XPS results indicate that the Cu^{2+} ions are incorporated into both tetrahedral and trigonal planar sites surrounded by S atoms in the hexagonal CuS crystal structure with a large internal space, whereas the Ni^{2+} ions are occupied by octahedral sites in the hexagonal NiS crystal system that will play an important role in the enhanced capability (see more detailed information in Fig. S1, ESI†), which are consistent with XRD results in Fig. 2f.

The electrochemical pseudo-capacitive behaviors of the HTMC-CS electrode were examined using cyclic voltammogram (CV) and galvanostatic charge/discharge measurements in a 1.0 M KOH electrolyte. Fig. 4a shows CV curves of the HTMC-CS electrode in a wide operating potential range from 0.0 to 0.7 V at a scan rate of 10 mV s^{-1}, exhibiting the typical pseudo-capacitive feature with a pair of strong symmetric redox peaks. It is suggested that the observed reversible redox pair is mainly related to Faradic redox reactions of NiS as follows:[26,27]

oxidation reaction (charge): $Ni^{2+}S + OH^- \rightarrow Ni^{3+}S(OH) + e^-$

reduction reaction (discharge): $Ni^{3+}S(OH) + e^- \rightarrow Ni^{2+}S + OH^-$

Here, note that although the CuS core material in HTMC-CS electrodes can naturally act as the

active site for the pseudo-capacitive behavior as reported in our previous work, the Faraday redox peak related to intercalation reaction of OH^- ions into CuS was not observed in this study due to its relatively low specific capacitance compared to NiS as indicated in the inset of Fig. 4a. To further investigate the reversible pseudo-capacitive behaviors of the HTMC-CS electrode, we carried out CV measurements with increasing scan rates from 5 to 50 mV s^{-1} as shown in Fig. 4b. It can be clearly seen that the all CV curves nearly retain their original curve shape with the redox pair of Ni^{2+}/Ni^{3+}, indicating the ideal pseudo-capacitive behavior and the high Faradic redox reaction reversibility.

To demonstrate the substantive electrochemical performance of the HTMC-CS electrode, the galvanostatic charge/discharge evaluation was carried out within a range of 0.0 and 0.5 V at different current densities ranging from 2 to 20 mA cm^{-2}, as shown in Fig. 4c. The HTMC-CS electrode exhibits a typical charge/discharge curve related to the reversible Faradic redox reactions between Ni^{2+}/Ni^{3+} with a high areal capacitance (700 mF cm^{-2} at 2 mA cm^{-2}). Moreover, the volumetric capacitance of the HTMC-CS electrode is found to be 25.9 F cm^{-3} at 2 mA cm^{-2}, which is considerably higher than that of previously reported pseudo-capacitive electrodes.[28-30] These results might be attributed to the unique nanoarchitecture structure with electrochemically active thin NiS shell layers existing on both the inner and outer surface of the electrically conductive tubular CuS core, allowing favaroble OH^- ion diffusion and low contact resistance as well as large electrolyte contact areas. Factually, we also confirmed that the HTMC-CS electrode exhibits a very low charge transfer resistance of 0.23 **Ω** from the Nyquist plot obtained by electrochemical impedance spectroscopy (EIS, Figs. 4d and S2a, ESI†). Moreover, we further showed that the diffusion coefficient (*D*) of OH^- ions in the HTMC-CS electrode is estimated to be 5.86×10^{-9} cm^2 s^{-1} from the Warburg impedance (see more detailed information in Fig. S2b, ESI†)[31-33], which is excellent when compared to the *D* of other reported pseudo-capacitive electrodes with a range of

10^{-10} ~ 10^{-12} cm^2 s^{-1} and lithium ion battery electrodes with a range of 10^{-11} ~ 10^{-16} cm^2 s^{-1}, as summarized in Table S1, ESI†. Thus, we believe that our unique hierarchical structure with the desirable core-shell electrode materials and geometry is beneficial to the charge transfer kinetics, playing an important role in determining the electrochemical performance and the cycling stability, as illustrated in Fig. 1b.

Moreover, it can be seen that the HTMC-CS electrode retains over 86.2% of its initial areal capacitance after repeating galvanostatic charge/discharge tests up to 2000 cycles at a current density of 10 mA cm^{-2}, as shown in Fig. S3, ESI†, indicating excellent capacitance retention capability. Additionally, we also observed that both the charge transfer resistance and the Warburg impedance related to the ion diffusion process almost remain unchanged with maintaining excellent capacitive nature (i.e., a phase angle is close to the ideal capacitor phase angle, -90° as shown in the inset of Fig. 4d) after 2000 cycles (Fig. 4d), demonstrating that the HTMC-CS electrode has the superior electrochemical stability during the charge/discharge process. This superior electrochemical stability can be attributed to the uniquely designed architecture with well-defined core-shell and hollow tubular structures, which can accommodate and relax mechanical stresses generated during the charge/discharge process, as indicated in Fig. 4e. Here, it should be further noted that the presence of an intermixed intermediate region between the CuS core and the NiS shell might significantly contribute to maintain the structural stability and integrity of the electrode. Thus, to understand in detail whether an energetically stable intermediate interlayer can be formed, we first carried out density-functional theory (DFT) calculations (see more detailed information in SI, ESI†). The structural models for the intermediate interlayer in the HTMC-CS were constructed based on $CuS_{(001)}$/$NiS_{(001)}$ planes between their hexagonal crystal structure (Fig. S4, ESI†). The calculations were performed with the assumption that Ni atoms are intermixed within the 1^{st} layer or 2^{nd} layer of the $CuS_{(001)}$/$NiS_{(001)}$ interface, as shown in Fig. 4f. The ratio of Ni atoms on the CuS

interface is denoted as interface intermixing from 0.00 to 1.00 monolayer (ML). It is found that the formation energy (ΔE) of all partial ML regions show negative values at both the 1st interlayer and the 2nd interlayer, indicating that Ni atoms can be partially intermixed with CuS to form an energetically stable intermediate state compared to the non-intermixing interface (0.00 ML). In contrast, the ΔE of 1.00 ML (fully covered with Ni atoms) has the positive formation energy, meaning the energetically unstable interface. Therefore, it is expected theoretically that the Ni atoms can be energetically intermixed within the CuS layer. Actually, the high-resolution TEM image of the HTMC-CS structure clearly shows that the interface between NiS and CuS has an intermediate interlayer region formed with Ni and Cu atoms during the synthesis process (Fig. S5a, ESI†). Furthermore, we clearly observed that the EDX line profiles of Ni and Cu not only show distinct shell and core regions, but also indicate the intermediate region with the mixed phase of Ni and Cu (Fig. S5b, ESI†), confirming the formation of an intermediate interlayer structure in the HTMC-CS, which can induce the enhanced adhesion and contact properties at the interface and hence leading to the improved structural stability.

To further understand core-shell structured hierarchy effects on electrochemically pseudo-capacitive kinetics in the HTMC-CS electrode, we additionally prepared the HTMC-CS with different NiS shell thicknesses under two different concentrations of Ni precursors with 0.5 and 2 M (denoted as HTMC-CS-L and HTMC-CS-H, respectively), as against the above discussed HTMC-CS (denoted as HTMC-CS-M) designed by an 1.0 M Ni precursor. Based on SEM, STEM, and EDX line-scanning analyses shown in Fig. S6, ESI†, we confirmed that NiS is coated along the wall of CuS nanotubes and the overall wall thickness of the HTMC-CS increases (decreases) with increasing (decreasing) the concentration of Ni precursors in comparison with HTMC-CS-M (Fig. 4a). As expected, it can be clearly seen that all CV curves of both electrodes with different shell thicknesses show a typical Faraday redox reaction of Ni^{2+}/Ni^{3+} similar to the CV curve in the

HTMC-CS-M electrode (Figs. S7a and S7b, ESI†). However, the HTMC-CS electrode exhibits an increase in the charge and discharge time with increasing the thickness of the NiS shell in the charge/discharge curves at the same current density, indicating that the areal and volumetric capacitance of the HTMC-CS-H electrode has the highest value compared to that of other HTMC-CS electrodes (Figs. 4c, S7c, S7d, and S8a, ESI†). To further address the role of the shell structure thickness in substantially affecting the pseudo-capacitive kinetics and the electrochemical performance of HTMC-CS electrodes, we also carried out EIS measurements to investigate OH^- ion diffusion behaviors and electrochemical stability in HTMC-CS electrodes with different shell thicknesses. As shown in Fig. 5a, the charge transfer resistance has a tendency to increase with gradually increasing the thickness of the NiS shell. In particular, the *D* of the HTMC-CS-M electrode, calculated from the Warburg impedance in Fig. S9, ESI†, is found to be 5.86×10^{-9} cm^2 s^{-1}, which is much larger than that of the HTMC-CS-H electrode (2.14×10^{-9} cm^2 s^{-1}). Moreover, as summarized in Fig. 5b, we found that the dynamic electrochemical behavior characteristics of the HTMC-CS electrodes, such as the rate performance and the cyclability, are significantly affected by the shell structure as a result of the dependence of the OH^- ions diffusivity and the effective charge transfer distance on the shell thickness, as shown in Fig. 5c. Accordingly, designing the shell structure with a proper thickness is important to maximize the pseudo-capacitive behaviors and electrochemical stability by considering the effective diffusion length of OH^- ions into the NiS shell layer, the intrinsic structural stability and capacity of NiS materials, and the effective electron transfer as well as the mechanical stress-mitigating interlayer between the NiS shell and the CuS core. Interestingly, we found that the HTMC-CS-M electrode exhibits the overall well-balanced electrochemical properties, such as the relatively improved high-rate retention and the high electrochemical cyclability with the high volumetric capacitance of 18.7 F cm^{-3} after 2000 cycling tests at a current density of 10 mA cm^{-2} (Fig. S8b, ESI†), which making it suitable for practical SC

applications.

In addition, to demonstrate the practical applicability of the well-engineered HTMC-CS-M electrode for SCs, an asymmetric SC (ASC) was fabricated using active carbon (AC) as an anodic electrode and the HTMC-CS-M as a cathodic electrode. In order to maximize energy storage performance in the ASC, we systemically designed and evaluated the AC anode electrode by carefully taking into account the overall charge balance between the two electrodes, as shown in Fig. S10, ESI†. From the CV curves of both the anode and cathode electrodes (Fig. 6a), it is estimated that the AC//HTMC-CS-M ASC can be operated within a wide operating potential window with a maximum working potential of 1.7 V. Furthermore, when the stable operating potential window is increased from 0.6 to 1.6 V with a step of 0.2 V at a scan rate of 50 mV s^{-1}, the ASC device exhibits a similar capacitive response without obvious distortion in the CV curves even in the operating potential of 1.6 V (Fig. 6b), showing the excellent charging/discharging capacitive characteristics. To further assess and quantify the electrochemical performance of the AC//HTMC-CS-M ASC, the galvanic charge/discharge measurements were carried out in the selected potential window of 1.6 V at different current densities ranging from 5 to 20 mA cm^{-2} (Fig. 6c). The volumetric capacitance of the ASC is estimated to be 7.44 F cm^{-3} at the current density of 5 mA cm^{-2}, which is much higher than that of other reported ASCs.[14,34-37] Moreover, the maximum volumetric power and energy densities of the device reach up to 770 mW cm^{-3} and 2.63 mWh cm^{-3}, respectively, as highlighted in the Ragone plot (Fig. 6d). Clearly, it can be seen that our ASC device exhibits much higher energy and power densities compared to previously reported other Ni-based and Cu-based ACSs and even exceeds the performance of the commercial SC device.[14,38-44] In addition to energy and power densities, the long-term cycling performance of SCs is another critical factor to be necessarily considered for practical applications. Fig. 6e shows the cyclability of our ASC device carried out at a current density of 10 mA cm^{-2} over the 10000 cycles. Noticeably, the ASC exhibits

the superior cycling stability with the capacitance retention of 84.0 % even after 10000 cycles, which explicitly demonstrates that our ACS device possesses the excellent electrochemical stability. Overall, the remarkably enhanced electrochemical properties of the AC//HTMC-CS-M ASC are mainly attributed to the well-engineered HTMC-CS nanoarchitectures with multiple synergistic benefits arising from the unique combination of core-shell material, geometry, and rational design.

CONCLUSIONS

We systematically designed and prepared the novel hierarchical transition metal chalcogenide architectures with a well-designed core-shell and hollow tubular structure for highly capable pseudo-capacitive SCs using a free-standing growth approach. We demonstrated that the resultant HTMC-CS structure is composed of highly conductive and structurally stable CuS core materials with the hollow tubular morphology, highly capacitive NiS shell materials with nanoscale thin layers on both the inner/outer surface of the CuS core, and energetically stable and good adhesive intermediate layers between the core and the shell. As a result, the optimized HTMC-CS electrodes displayed a remarkably superior volumetric capacitance of 25.9 F cm^{-3} at a current density of 2 mA cm^{-2} and good rate performance as well as excellent capacitance retention capability. This result might be attributed to the large electrolyte contact areas, the effective diffusion route and distance of OH^- ions, the high electrical conductivity and low charge transfer resistance, and the mechanical stress-mitigating interlayer and tubular strucure, arising from the combined synergistic benifits of the unique hierarchical architecture with the combination of core-shell structure and materials. Furthermore, we also demonstrated that the AC//HTMC-CS-M ASC exhibits the outstanding electrochemical performance with high power (770 mW cm^{-3}) and energy (2.63 mWh cm^{-3}) densities and ultrahigh reversible cyclability (capacitance retention of 84%) during 10000 cycles.

EXPERIMENTAL

Fabrication of HTMC-CS nanoarchitectures

Copper hydroxide ($Cu(OH)_2$ nanotubes were synthesized directly on the Cu mesh (1 x 1 cm^2 with a thickness of 0.0267 cm, Alfa Aesar) by immersing into the solution with 10 M sodium hydroxide (NaOH, 10 mL), 1 M ammonium persulfate ($(NH_4)_2S_2O_8$, 5 mL) and DI water (22.5 mL). CuS nanotube arrays were then fabricated through the sulfurization of the pre-synthesized $Cu(OH)_2$ nanotubes with 0.2 M thiourea (CH_4N_2S) and subsequent annealing process at 150 ^oC, as described in our previous report.[14] After that, HTMC-CS nanoarchitectures with the NiS/CuS core-shell nanotubes were obtained by the following sequences: sequential dipping CuS nanotube samples in (a) nickel(II) chloride hexahydrate ($NiCl_2 \cdot 6H_2O$) solutions and (b) thiourea solutions with different concentrations, 0.5, 1, and 2 M (denoted as HTMC-CS-L, HTMC-CS-M, and HTMC-CS-H, respectively). The samples were subsequently blow dry with nitrogen gas and then annealed on a hot plate at 150 ^oC.

Electrochemical Characterization

The electrochemical properties of the HTMC-CS nanostructure directly grown on the Cu mesh were measured in a three-electrode system based on the HTMC-CS electrodes as a working electrode using a potentiostat (PGSTAT302N, Metrohm, Autolab). For the fabrication of anode electrodes in the ASC, the slurry was prepared by mixing active carbon as an active material, poly(vinylidene difluoride) as a binder, and Ketjen black as a conductive material, and then was coated onto the compressed nickel foam as a current collector. All electrochemical analyses of the AC//HTMC-CS-M ASC were performed using a two electrode system under a 1.0 M KOH solution at room temperature.

Acknowledgments

This research was supported by the Industrial Fundamental Technology Development Program (10052745, Development of nano-sized (100 nm) manganese ceramic material for high voltage pseudo-capacitor) funded by the Ministry of Trade, Industry and Energy (MOTIE) of Korea, and the European Research Council under the European Union's Seventh Framework Programme (FP/2007-2013)/Grant Agreement no. 685758, Project '1D-NEON'.

Author contribution

Y.-W.L., B.-S.K. and J.I.S. planned this research and wrote the manuscript. Y.-W.L. and B.-S.K. carried out the preparation of THMC-CS nanoarchitectures and their electrochemical analyses. H.C. performed the DFT calculation. J.H., S.P., J.L. and S.-H.L. analyzed and discussed the structural and chemical characteristics of the material. J.P.H. carried out the XRD analysis. B.H., H.-S.J., D.W. and H.S.S. performed the TEM and EDX analyses. S.M.M., S.N.C. and J.M.K. contributed to the interpretation of the data and commented on the manuscript.

References

[1] G. Wang, L. Zhang and J. Zhang, *Chem. Soc. Rev.*, 2012, **41,** 797–828.

[2] P. Simon, Y. Gogotsi and B. Dunn, *Science*, 2014, **343,** 1210–1211.

[3] C. Wu and Y. Xie, *Adv. Mater.*, 2015, **27,** 3850–3867.

[4] Z. Yu, L. Tetard, L. Zhai and J. Thomas, *Energy Environ. Sci.*, 2015, **8,** 702–730.

[5] J. Shi , X. Li, G. He , L. Zhang and M. Li, *J. Mater. Chem. A*, 2015, **3,** 20619–20626.

[6] J. Cai, Z. Li and P. K. Shen, *ACS Appl. Mater. Interfaces*, 2012, **4,** 4093–4098.

[7] R. Ramachandran, M. Saranya, P. Kollu, B. P. C. Raghupathy, S. K. Jeong and A. N. Grace, *Electrochim. Acta*, 2015, **178,** 647–657.

[8] X. Li, J. Shen, N. Li and M. Ye, *J. Power Sources*, 2015, **282,** 194–201.

[9] J. Yang, X. Duan, Q. Qin and W. Zheng, *J. Mater. Chem. A*, 2013, **1,** 7880–7884.

[10] X. Yan, X. Tong, L. Ma, Y. Tian, Y. Cai, C. Gong, M. Zhang and L. Liang, *Mater. Lett.*, 2014, **124,** 133–136.

[11] J. Yang, X. Duan, W. Guo, D. Li, H. Zhang and W. Zheng, *Nano Energy*, 2014, **5,** 74–81.

[12] J. Wu, C. Ouyang, S. Dou and S. Wang, *Nanotechnol.*, 2015, **26,** 325401.

[13] D. Ghosh and G. K. Das, *ACS Appl. Mater. Interfaces*, 2015, **7,** 1122–1131.

[14] Y.-W. Lee, B.-S. Kim, J. Hong, J. Lee, S. Pak, H.-S. Jang, D. Whang, S. N. Cha, J. I. Sohn and J. M. Kim, *J. Mater. Chem. A*, 2016, **4,** 10084–10090.

[15] J. Yang, X. Duan, Q. Qin and W. Zheng, *J. Mater. Chem. A*, 2013, **1,** 7880−7884.

[16] H. Peng, G. Ma, K. Sun, J. Mu, H. Wang and Z. Lei, *J. Mater. Chem. A*, 2014, **2,** 3303−3307.

[17] H. Geng, S. F. Kong and Y. Wang, *J. Mater. Chem. A*, 2014, **2,** 15152−15158.

[18] M. H. Kunita, E. M. Girotto, E. Radovanovic, M. C. Goncalves, O. P. Ferreira, E.C. Muniz and A. F. Rubira, *Appl. Surf. Sci.*, 2002, **202,** 223−231.

[19] Investing in Mining Stocks, Metals and Commodities, http://www.infomine.com/investment,

(accessed 29 September 2016).

[20] T. Zhu, H. B. Wu, Y. Wang, R. Xu and X. W. Lou, *Adv. Energy Mater.*, 2012, **2,** 1497–1502.

[21] Z. Xing, Q. Chu, X. Ren, C. Ge, A. H. Qusti, A. M. Asiri, A. O. Al-Youbi and X Sun, *J. Power Sources*, 2014, **245,** 463–467.

[22] Q. Chu, W. Wang, X. Wang, B. Yang, X. Liu and J. Chen, *J. Power Sources*, 2015, **276,** 19–25.

[23] J. F. Moulder, W. F. Stickle, P. E. Sobol and K. D. Bomben, *Handbook of X-ray photoelectron spectroscopy*, 1995, Physical Electronics, Inc., Minnesota.

[24] L. Chen, J. He, Q. Yuan, Y.-W. Zhang, F. Wang, C.-T. Au and S.-F. Yin, *RSC Adv.*, 2015, **5,** 33747–33754.

[25] R. Bhosale, S. Kelkar, G. Parte, R. Fernandes, D. Kothari and S. Ogale, *ACS Appl. Mater. Interfaces*, 2015, **7,** 20053–20060.

[26] S.-W. Chou and J.-Y. Lin, *J. Electrochem. Soc.*, 2013, **160,** D178–D182.

[27] P. Hao, J. Tian, Y. Sang, C.-C. Tuan, G. Cui, X. Shi, C. P. Wong, B. Tang and H. Liu, *Nanoscale*, 2016, **8,** 16292–16301.

[28] H.-J. Ahn, W. B. Kim and T.-Y. Seong, *Electrochem. Commun.*, 2008, **10,** 1284–1287.

[29] Y. Jiang, P. Wang, X. Zang, Y. Yang, A. Kozinda and L. Lin, *Nano Lett.*, 2013, **13,** 3524–3530.

[30] W. Sun, R. Zheng and X. Chen, *J. Power Sources*, 2010, **195,** 7120–7125.

[31] H.-C. Park, K.-H. Lee, Y.-W. Lee, S.-J. Kim, D.-M. Kim, M.-C. Kim and K.-W. Park, *J. Power Sources*, 2014, **269,** 534–541.

[32] Y.-W. Lee, D.-M. Kim, S.-J. Kim, M.-C. Kim, H.-S. Choe, K.-H. Lee, J. I. Sohn, S. N. Cha, J. M. Kim and K.-W. Park, *ACS Appl. Mater. Interfaces*, 2016, **8,** 7022–7029.

[33] Y.-W. Lee, G.-H. An, B.-S. Kim, J. Hong, S. Pak, E.-H. Lee, Y. Cho, J. Lee, P. Giraud, S. N. Cha, H.-J. Ahn, J. I. Sohn and J. M. Kim, *ACS Appl. Mater. Interfaces*, 2016, **8,** 17651–17658.

[34] X. Lu, M. Yu, T. Zhai, G. Wang, S. Xie, T. Liu, C. Liang, Y. Tong and Y. Li, *Nano Lett.,* 2013, **13,** 2628–2633.

[35] T. Zhai, F. Wang, M. Yu, S. Xie, C. Liang, C. Li, F. Xiao, R. Tang, Q. Wu, X. Lu and Y. Tong, *Nanoscale,* 2013, **5,** 6790–6796.

[36] X. Lu, M. Yu, G. Wang, T. Zhai, S. Xie, Y. Ling, Y. Tong and Y. Li, *Adv. Mater.,* 2013, **25,** 267–272.

[37] M. Yu, W. Wang, C. Li, T. Zhai, X. Lu and Y. Tong, *NPG Asia Mater.*, 2014, **6,** e129.

[38] D. Yu, K. Goh, H. Wang, L. Wei, W. Jiang, Q. Zhang, L. Dai and Y. Chen, *Nat. Nanotechnol.*, 2014, **9,** 555–562.

[39] X. Xiao, T. Li, P. Yang, Y. Gao, H. Jin, W. Ni, W. Zhan, X. Zhang, Y. Cao, J. Zhong, L. Gong, W.-C. Yen, W. Mai, J. Chen, K. Huo, Y.-L. Chueh, Z. L. Wang and J. Zhou, *ACS Nano,* 2012, **6,** 9200–9206.

[40] X. Lu, D. Zheng, T. Zhai, Z. Liu, Y. Huang, S. Xie and Y. Tong, *Energy Environ. Sci.*, 2011, **4,** 2915–2921.

[41] W. Chen, R. B. Rakhi and H. N. Alshareef, *J. Mater. Chem.*, 2012, **22,** 14394–14402.

[42] Z.-S. Wu, W. Ren, D.-W. Wang, F. Li, B. Liu and H.-M. Cheng, *ACS Nano,* 2010, **4,** 5835–5842.

[43] W. Zilong, Z. Zhu, J. Qiu and S. Yang, *J. Mater. Chem. C*, 2014, **2,** 1331–1336.

[44] P. Yang, X. Xiao, Y. Li, Y. Ding, P. Qiang, X. Tan, W. Mai, Z. Lin, W. Wu, T. Li, H. Jin, P. Liu, J. Zhou, C.P. Wong, Z.L. Wang, *ACS Nano,* 2013, **7,** 2617–2626.

Fig. 1 Y.–W. Lee *et al.*

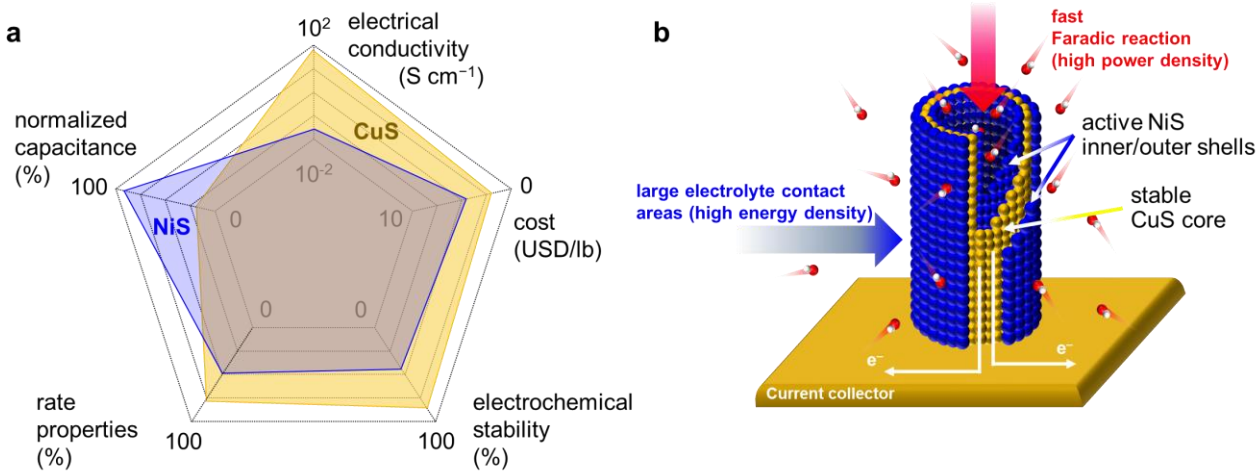

Fig. 1 (a) Radar plots to present the important factors of NiS and CuS for evaluating the combination of core-shell materials in pseudo-capacitive SCs. (b) Schematic illustration for the synergistic effects of the proposed hierarchical transition metal (Cu and Ni) chalcogenide core-shell electrode on electrochemical behavior and performance.

Fig. 2 Y.–W. Lee *et al.*

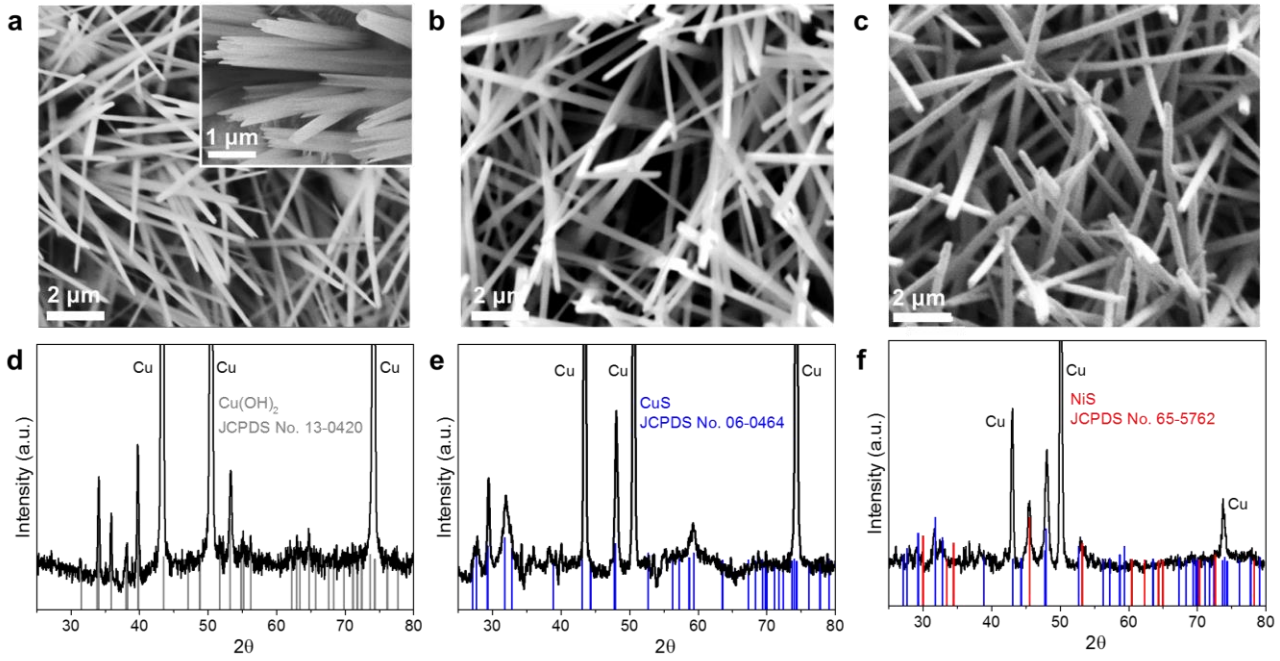

Fig. 2. SEM images of (a) $Cu(OH)_2$ nanotubes, (b) CuS nanotubes, and (c) HTMC-CS nanoarchitectures prepared by hierarchical bottom-up synthetic processes. The inset in Fig. 1a clearly shows that the tip of $Cu(OH)_2$ nanotubes is open. XRD patterns of (a) $Cu(OH)_2$ nanotubes, (b) CuS nanotubes, and (c) HTMC-CS nanoarchitectures.

Fig. 3 Y.–W. Lee *et al.*

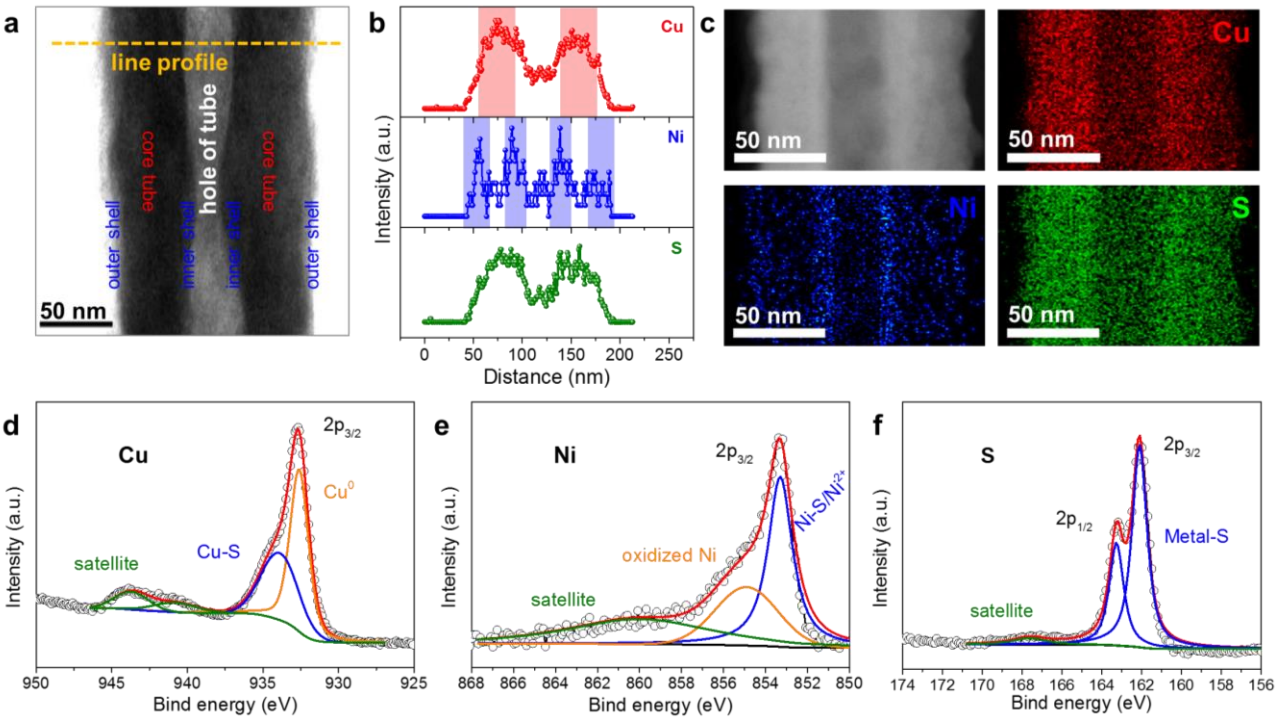

Fig. 3 (a) TEM images, (b) EDX line-scanning profiles, and (c) scanning TEM (STEM) and EDX mapping images for the Cu (red), Ni (blue), and S (green) in the HTMC-CS nanostructure. XPS (d) Cu, (e) Ni, and (f) S spectra of the HTMC-CS nanostructure.

Fig. 4 Y.–W. Lee *et al.*

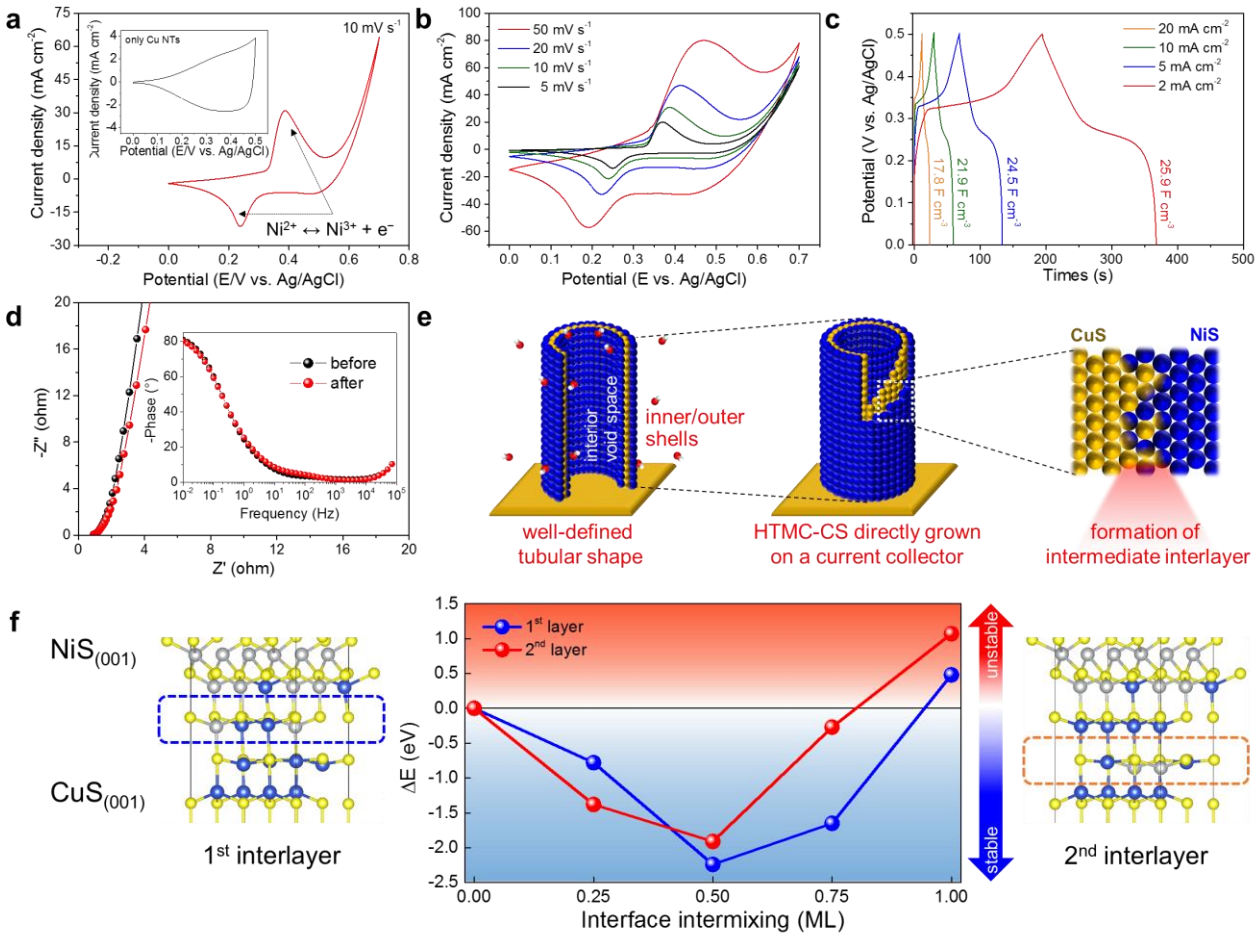

Fig. 4 (a) CV curves of the HTMC-CS electrode at 10 mV s^{-1} in a 1.0 M KOH electrolyte. The inset indicates the CV curve of the CuS electrode]. (b) CV curves of the HTMC-CS electrode at different scan rates from 5 to 50 mV s^{-1}. (c) Galvanostatic charge/discharge curves of the HTMC-CS electrode at different current densities from 2 to 20 mA cm^{-2}. (d) Nyquist plots of the HTMC-CS electrode before and after cycling tests. The inset indicates Bode plots. (e) Schematic illustration related to the structural benefits, allowing the enhanced electrochemical stability in the HTMC-CS electrode. (f) Calculated formation energy (ΔE) for interface intermixing in $CuS_{(001)}/NiS_{(001)}$ planes using DFT calculations. Images of optimized intermixed structure on the 1st interlayer (left) and 2nd interlayer (right).

Fig. 5 Y.–W. Lee *et al.*

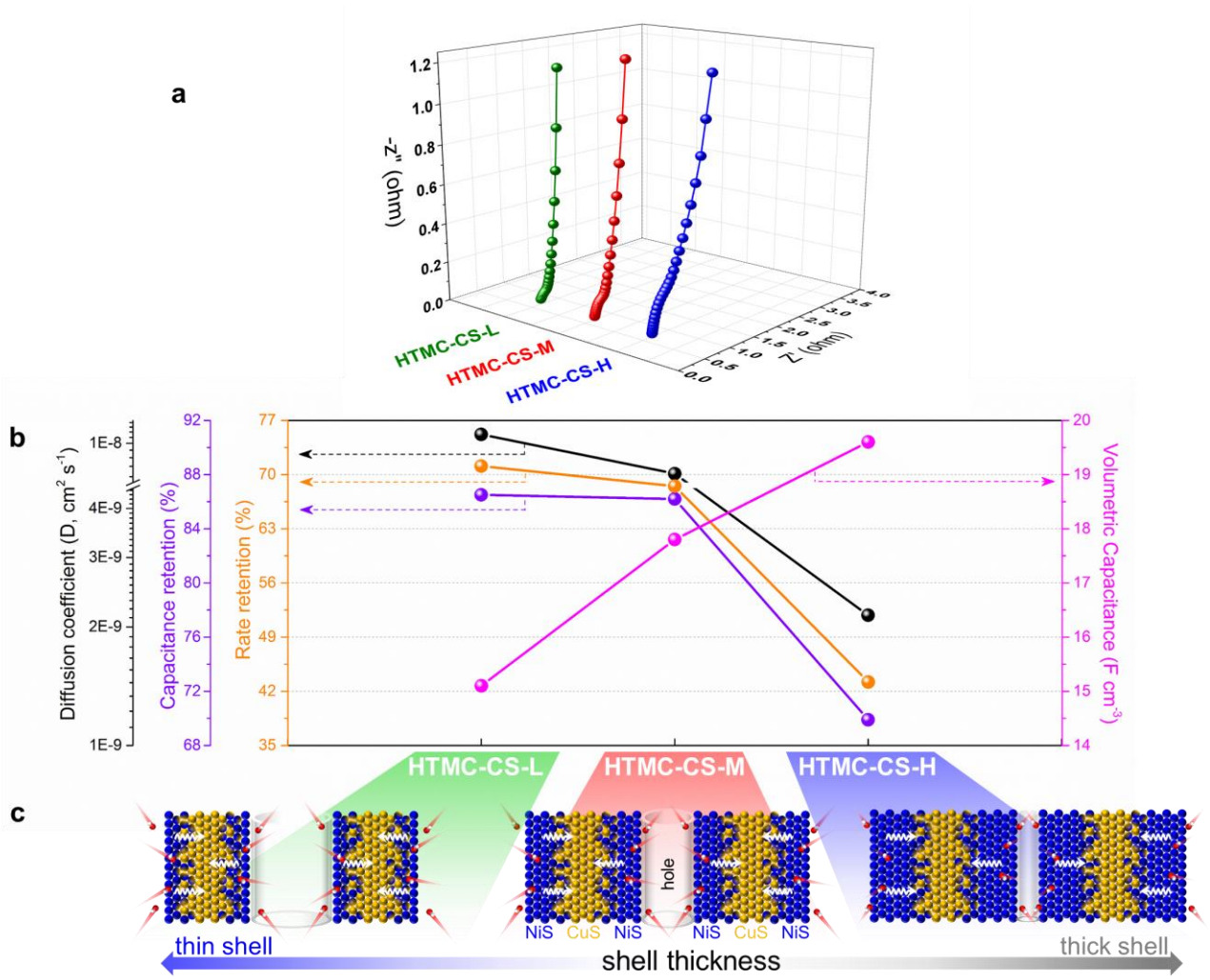

Fig. 5 (a) Nyquist plots of all three different HTMC-CS electrodes. (b) The comparison of various electrochemical performances such as diffusion coefficient, capacitance and rate retentions, and volumetric capacitance for all HTMC-CS electrodes. These electrochemical parameters are obtained from the results shown in Figs. S8 and S9, ESI†. (c) Schematic illustration of dynamic pseudo-capacitive behavior characteristics of HTMC-CS electrodes with different shell thicknesses.

Fig. 6 Y.–W. Lee *et al.*

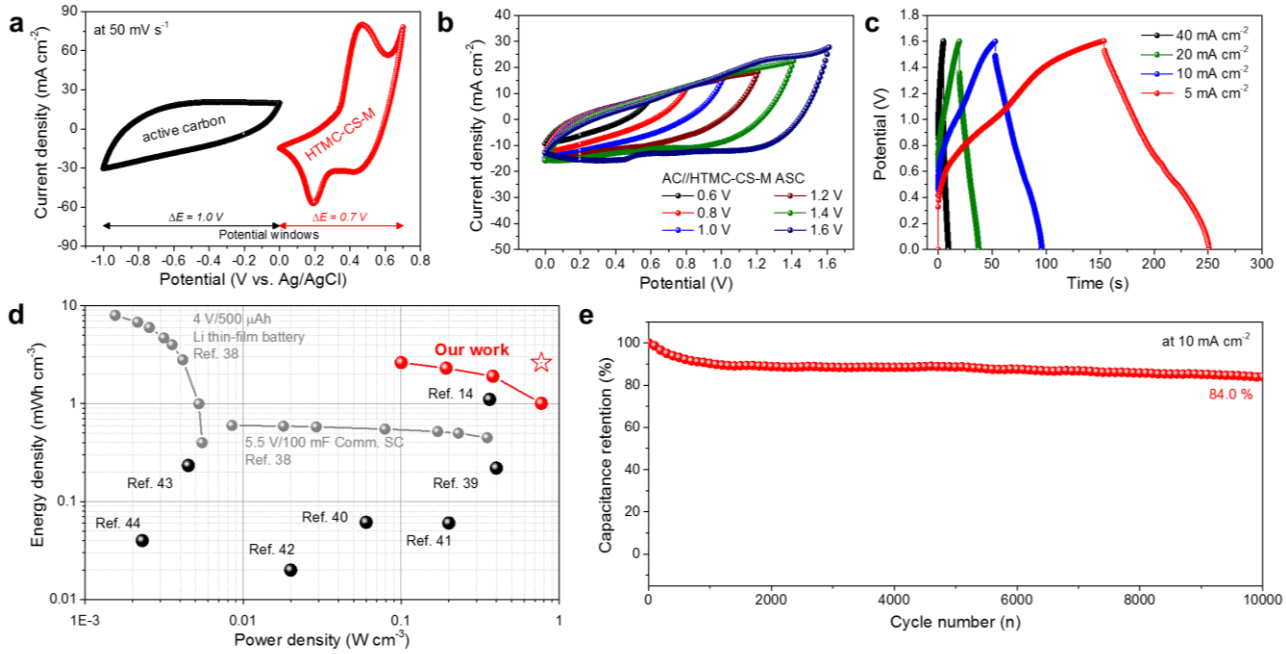

Fig. 6 (a) Comparative CV curves of AC and HTMC-CS-M at 50 mV s^{-1}. (b) CV curves of the AC//HTMC-CS-M ASC in different upper potentials from 0.6 to 1.6 V at a scan rate of 50 mV s^{-1}. (c) Galvanostatic charge/discharge curves of the ASC under various different current densities. (d) Ragone plots related to energy and power densities of the AC//HTMC-CS-M ASC for a comparison with recently reported other pseudo-capacitive SCs. (e) Cycling performance of the ASC at a current density of 10 mA cm^{-2} up to 10000 cycling charge/discharge tests.